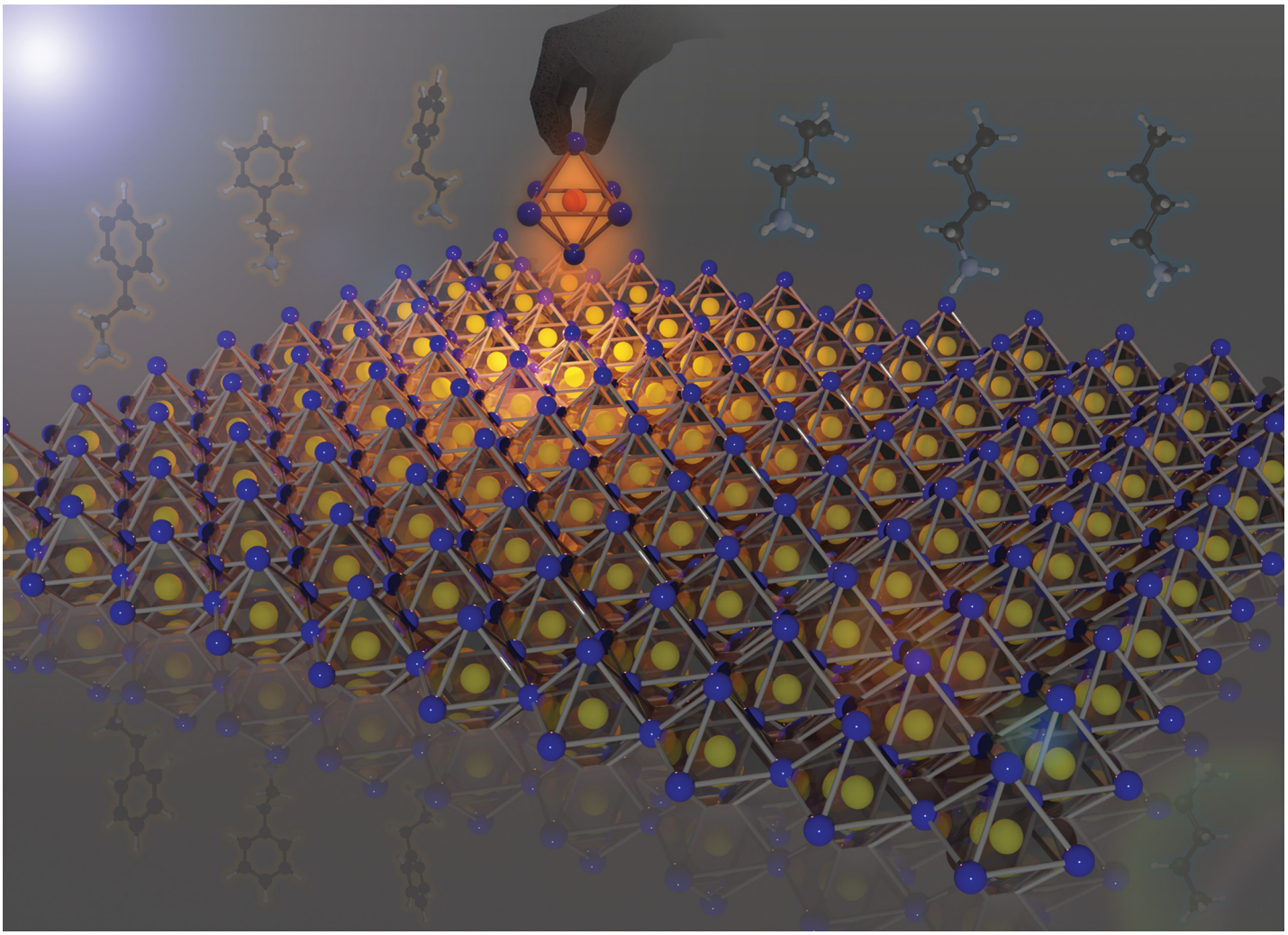

Showcasing research from Professor Gangishetty's laboratory, Department of Chemistry, Mississippi State University, Mississippi, USA.

Interstitial and substitutional doping of Mn^{2+} in 2D PEA_2PbBr_4 and BA_2PbBr_4 perovskites

This work provides comprehensive structural analyses of the type of Mn^{2+} doping, interstitial *vs.* substitutional, in 2D PEA_2PbBr_4 and 2D BA_2PbBr_4 perovskite hosts. Furthermore, the doping type is linked to optical properties such as exciton diffusion and dopant-to-host energy transfer.

As featured in:

See Ferry Prins, Mahesh K. Gangishetty *et al.*, *Chem. Commun.*, 2024, **60**, 14960.

ROYAL SOCIETY OF CHEMISTRY

rsc.li/chemcomm

Registered charity number: 207890

ChemComm

COMMUNICATION

View Article Online
View Journal | View Issue

Cite this: *Chem. Commun.*, 2024, **60**, 14960

Received 10th August 2024,
Accepted 10th October 2024

DOI: 10.1039/d4cc04074k

rsc.li/chemcomm

Interstitial and substitutional doping of Mn^{2+} in 2D PEA_2PbBr_4 and BA_2PbBr_4 perovskites†

Udara M. Kuruppu,[a] Alvaro J. Magdaleno,[cd] Anuraj S. Kshirsagar,[a] Bruno Donnadieu,[a] Ferry Prins *[cd] and Mahesh K. Gangishetty *[ab]

Mn^{2+} doping imposes intriguing optoelectronic properties on lead-halide perovskites; however, its impact on their crystal structure remains unclear. This study investigates the consequences of interstitial and substitutional Mn^{2+} doping on the lattice-strain and interplanar spacings of 2D perovskites and correlates the structural changes to their optical properties.

Doping with a foreign metal ion is an attractive strategy to improve the properties of semiconductors such as lead-halide perovskites. Due to the flexible nature of perovskite structures, a wide range of metal ions have been explored. Among these, Mn^{2+} has been most extensively studied due to its bright characteristic emission and paramagnetic nature.[1,2] Despite these extensive studies, the nature of Mn^{2+} doping such as interstitial or substitutional, and the role of host lattice on the doping is still ambiguous. There have been several contradicting results reported on the type of Mn^{2+} doping. Some reports showed lattice contraction due to substitutional Mn^{2+} doping, while others demonstrated lattice expansion owing to their interstitial nature. Generally, the lattice expansion and contraction can be identified by the shift in their p-XRD peaks. Recently, Torma *et al.* observed a shift in the XRD peak to lower angles and demonstrated interstitial Mn^{2+} doping in $Cs_2PbI_2Cl_2$ using nano-XRD and nano-XRF measurements.[3] On the contrary, Dutta *et al.* and Hou *et al.* observed a peak shift to the higher angles in XRD after doping with Mn^{2+} in 2D Cs_2PbBr_4 nanoplatelets and 3D $CsPb(BrCl)_3$ perovskite nanocrystals.[4,5] Interestingly, Nag *et al.* observed no shift in the XRD peak when Mn^{2+} (<1%) is doped in 2D BA_2PbBr_4 perovskite.[6] Therefore, a comprehensive understanding of the nature of doping, its dependence on the host lattice structure, and its impact on the crystal structure, lattice strain, and optical properties of perovskites is required.

In this study, we utilize Mn^{2+} doping in two different 2D perovskite hosts: (i) phenylethylammonium lead bromide (PEA_2PbBr_4) and (ii) butylammonium lead bromide (BA_2PbBr_4), to investigate their structural changes and link these changes to their optical properties. These two perovskites are selected by considering the difference in their structural rigidity owing to the difference in their A-site ions, although both adopt similar layered 2D structures of the Ruddlesden–Popper (RP) type.[7] Consequently, our study reveals that the nature of Mn^{2+} doping is significantly different in both PEA_2PbBr_4 and BA_2PbBr_4. We observed a striking difference in their XRD patterns after Mn^{2+} doping. PEA_2PbBr_4 showed lattice expansion perpendicular to the plane of the 2D inorganic framework (interstitial nature) after doping with Mn^{2+} whereas BA_2PbBr_4 showed a lattice contraction along the 2D plane (substitutional doping). Due to the manifestation of a soft lattice with a layered structure of 2D perovskites, the Mn^{2+} doping was feasible, and the changes in their crystal structure were easily noticeable after Mn^{2+} incorporation. Subsequently, this resulted in a dramatic difference in their emission; orange (Mn^{2+}) emission in Mn^{2+}:PEA_2PbBr_4 is more intense (~10× higher) than that of Mn^{2+}:BA_2PbBr_4. Upon tracking the exciton diffusion using transient photoluminescence microscopy (TPLM), we found that the exciton transport in PEA_2PbBr_4 is unaffected, whereas a noticeable difference in the exciton transport was observed in BA_2PbBr_4 with Mn^{2+} doping.

To commence our study, undoped and a series of Mn^{2+} doped 2D perovskites were synthesized using acid-initiated precipitation (detailed methodology is available in the ESI†). The ICP-MS analyses reveal that the amount of Mn^{2+} increases with an increase in the concentration of Mn^{2+} salts in the precursors (shown in Table S3, ESI†). However, the maximum feasible doping amount was 4.8% and 2.0% of Mn^{2+} (respective to the molar percentage of Pb^{2+}) for PEA_2PbBr_4 and BA_2PbBr_4, respectively. Such low

[a] *Department of Chemistry, Mississippi State University, Mississippi State, Mississippi 39762, USA. E-mail: mg2234@msstate.edu*
[b] *Department of Physics and Astronomy, Mississippi State University, Mississippi State, Mississippi 39762, USA*
[c] *Condensed Matter Physics Center (IFIMAC), Autonomous University of Madrid, 28049, Madrid, Spain. E-mail: ferry.prins@uam.es*
[d] *Department of Condensed Matter Physics, Autonomous University of Madrid, 28049, Madrid, Spain*

† Electronic supplementary information (ESI) available. See DOI: https://doi.org/10.1039/d4cc04074k

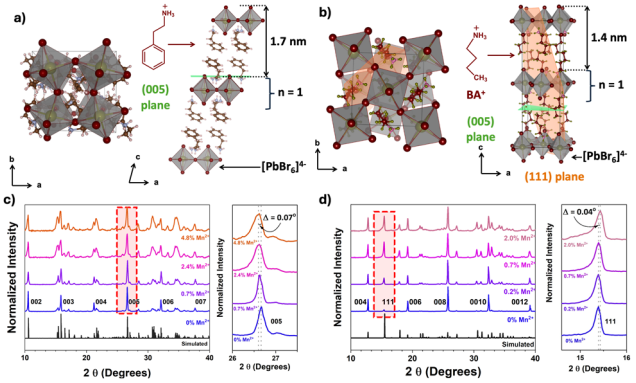

Fig. 1 Crystal structures of (a) PEA_2PbBr_4 and (b) BA_2PbBr_4. The pXRD patterns of undoped and Mn^{2+} doped (c) PEA_2PbBr_4 and (d) BA_2PbBr_4. The 2D perovskite lattices of PEA_2PbBr_4 and BA_2PbBr_4 are composed of a single (n = 1) inorganic layer of $[PbBr_6]^{4-}$ octahedra. The PEA^+ and BA^+ cations act as organic spacers between the octahedral layers of PEA_2PbBr_4 and BA_2PbBr_4, respectively.

doping levels of Mn^{2+} are attributed to a difference in the ionic radii of Mn^{2+} (0.83 Å) compared to that of Pb^{2+} (1.19 Å).[6,8] The crystal structures of PEA_2PbBr_4 and BA_2PbBr_4 were analyzed by scXRD and shown in Fig. 1a and b (see Tables S1 and S2 for refined data, ESI†). Both perovskites show 2D layered Ruddlesden–Popper (RP) type structures and exhibit a higher degree of preferential orientation along the c-axis. Further, their p-XRD patterns were recorded after doping with various amounts of Mn^{2+} (Fig. 1c and d), which was and used for strain analyses. From p-XRD, we found that both perovskites retain the RP structures even after doping with Mn^{2+}.

In the case of PEA_2PbBr_4, both undoped and Mn^{2+} doped perovskites show equally spaced and sharp diffraction peaks in p-XRD (Fig. 1c), denoted as (002), (003), (004), *etc.*, and agree with the simulated pattern of a triclinic phase (lattice parameters $a \neq b \neq c$, $\alpha \neq \beta \neq \gamma$) derived from scXRD. All these peaks arise from the same family of planes $\{00l\}$ where ($l = n$), indicating the high degree of orientation with stacking layers. The periodic peaks due to these ($00l$) diffractions imply the spacing between the two layers, since these planes are perpendicular to the stacking axis (c-axis), see Fig. 1a. The periodicity obtained from the diffraction peaks was 1.648 ± 0.007 nm, indicating that each layer is ~1.65 nm apart, as shown in Fig. 1a. After doping with Mn^{2+}, no major changes in the p-XRD pattern were observed; however, a shift in some XRD peaks with slight broadening was observed. These peaks are at ~26.6° and at ~37.6°, which correspond to the (005) plane and the (007) plane, respectively, as shown in the magnified region of Fig. 1c and Fig. S1 (ESI†). The magnitude of the shift was $\Delta 2\theta_{005} = 0.07°$ and $\Delta 2\theta_{007} = 0.09°$. Generally, given the difference in the ionic radii of Pb^{2+} (1.19 Å) and Mn^{2+} (0.83 Å), if Pb^{2+} is replaced by smaller Mn^{2+}, a lattice contraction is expected with a shift in the XRD peaks to higher angular scale. On the contrary, in this case, the XRD peaks shifted to lower angles, indicating that there is a lattice expansion after doping with Mn^{2+} ions. This also implies that the Mn^{2+} ions are not replacing Pb^{2+}. Since this shift is observed for (005) and (007) peaks, the lattice expansion occurs in an out-of-plane direction (perpendicular to (005) and (007) planes) along the c-axis, as shown in Fig. 1a. This is also evident from an increase in the spacing of (005) planes, as shown in Fig. 2a. Similar trends in p-XRD were observed by Torma *et al.*[3] By using nano-XRD, they demonstrated that Mn^{2+} occupies the interstitial position.[3]

In the case of 2D BA_2PbBr_4, the powder XRD patterns of both undoped and Mn^{2+} doped show equally spaced and sharp diffraction peaks indexed as (002), (004), (006), *etc* (Fig. 1d). This diffraction pattern aligns well with the simulated pattern obtained from the reference and scXRD data, confirming the orthorhombic Ruddlesden–Popper crystal structure (lattice parameters $a \neq b \neq c$, $\alpha = \beta = \gamma = 90°$). All these peaks arise from the same family of planes $\{00l\}$, where ($l = 2n$) indicates highly oriented crystallites. The periodicity, obtained from $\{00l\}$ family peaks, was found to be 1.366 ± 0.008 nm. Note that this interlayer spacing is smaller than the spacing in PEA_2PbBr_4 perovskite. Unlike PEA_2PbBr_4, neither a peak shift nor broadening of the ($00l$) planes was observed upon doping, indicating these planes are unaffected after the incorporation of Mn^{2+} in BA_2PbBr_4. Interestingly, in addition to the ($00l$) family peaks, another peak at ~15.5°, corresponds to the (111) plane, was observed (Fig. 1d). This (111) plane cuts the organic and inorganic layers diagonally, as shown in Fig. 1b.[9] Upon a close examination, a slight shift in the ~15.5° peak to higher angles was observed (magnified region of Fig. 1d). This shift was more prominent at higher (>1%) Mn^{2+} doping, and almost negligible at lower doping levels. The magnitude of this shift was $\Delta 2\theta = 0.04°$. The shift in this peak to higher angular scale implies there is a lattice contraction along the out-of-plane direction along the *ab*-plane (perpendicular to the (111) plane and the c-axis), as shown in Fig. 1b. This is further corroborated by the decrease in d-spacing of (111) planes, as shown in Fig. 2b. From the crystal structure in Fig. 1b, this *ab* plane represents the plane of the inorganic framework; the lattice contraction along this plane implies that there is shrinkage of the inorganic framework. This is possible only when the central atom, Pb^{2+}, is replaced by an atom with a smaller ionic radius such as Mn^{2+}. Therefore, from these analyses, it is evident that the Mn^{2+} in BA_2PbBr_4 is substituting Pb^{2+}, whereas, in the case of PEA_2PbBr_4, the Mn^{2+} is occupying interstitial sites.[6,10] This difference in occupancy, despite the similar layered RP type structure, could be attributed to either the smaller interlayer spacing in BA_2PbBr_4 compared to PEA_2PbBr_4 or a difference in the lattice

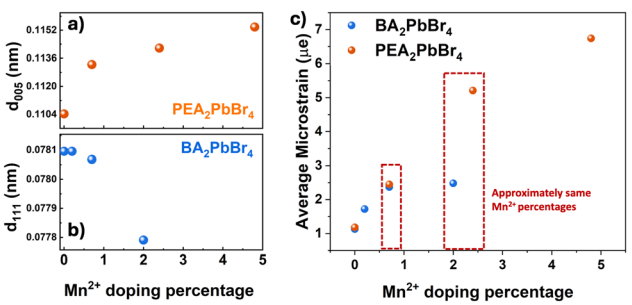

Fig. 2 The change in d-spacing against Mn^{2+} concentration of (a) the (005) plane in PEA_2PbBr_4 (b) the (111) plane in BA_2PbBr_4 and (c) microstrain *vs.* Mn^{2+} doping percentage.

rigidity owing to difference in their organic spacers (aromatic *vs.* aliphatic). Perhaps this substitutional nature of Mn^{2+} doping is limiting the amount of Mn^{2+} that can be incorporated into BA_2PbBr_4, since a maximum of only ~2% doping was achievable synthetically.

Regardless of the crystal phases, type of spacers, and interstitial or substitutional doping, the incorporation of Mn^{2+} into the perovskite host can induce strain in the lattice. Generally, from the changes in the p-XRD peaks, one can estimate the strain in the lattice. A peak shift with a slight broadening in PEA_2PbBr_4 after Mn^{2+} doping may be an indication of a homogenous strain caused by the uniform expansion of the lattice. Whereas a moderate change in peak position in the case of BA_2PbBr_4, suggesting that the magnitude of the lattice strain is less in the case of BA_2PbBr_4.[11] To quantitatively compare the microstrain induced by Mn^{2+} incorporation in these two host lattices, we employed the Williamson–Hall method (Fig. S2, ESI†).[12] A Voigt function, which is convoluted Lorentzian and Gaussian functions, was used to fit the p-XRD peaks and derive the FWHM for the strain analyses. From Fig. 2c, a striking difference in the microstrain was observed at higher Mn^{2+} levels. At >2% of Mn^{2+} doping, the strain in the PEA_2PbBr_4 is approximately three times higher than that of BA_2PbBr_4, implying that the interstitial doping can induce more strain in the lattice than the substitutional doping.

Next, the impact of these discrepancies in the Mn^{2+} occupancy on the optical properties of perovskites was investigated. We recorded absorption, photoluminescence (PL), and exciton diffusion in PEA_2PbBr_4 and BA_2PbBr_4 perovskites with and without Mn^{2+} doping. As shown in Fig. S3 (ESI†), both pristine perovskites exhibit sharp excitonic features in the UV-vis absorption spectra with similar band-edge absorption at 2.89 eV (430 nm) for PEA_2PbBr_4 and at 2.85 eV (435 nm) for BA_2PbBr_4 (Fig. S4, ESI†). The absorbance remains unchanged upon Mn^{2+} doping of the pristine 2D perovskites. Supporting this, we observed no change in the excitation (PLE) spectra after Mn^{2+} doping (Fig. S6, ESI†). The PL spectra of both pristine 2D perovskites exhibit two emission features around 410 nm and 430 nm, similar to other studies.[13] As these are 2D layered perovskites, the lower energy peak at 430 nm is due to the recombination of edge excitons, while the higher energy transition at 410 nm is designated to interior excitons.[10,13] When Mn^{2+} is introduced into both BA_2PbBr_4 and PEA_2PbBr_4, a new broad, intense emission at 600 nm was observed. This 600 nm emission has been assigned to $^4T_{1g} \rightarrow {}^6A_{1g}$ d–d transition in Mn^{2+}.[6,10] These Mn states are typically sensitized from the host's excitation, and the emission originates from the excitonic energy transfer from the host to the dopant ion (Fig. S5, ESI†).[6] Interestingly, the intensity of the Mn^{2+} peak (600 nm) with respect to the host peak (~430 nm) is significantly different in Mn^{2+}:BA_2PbBr_4 compared to Mn^{2+}:PEA_2PbBr_4 (Fig. S7, ESI†); this is true even in the case of samples with the same amount of Mn^{2+} (Fig. S13, ESI†). For instance, the PL intensity ratio between dopant and host emission in ~2% Mn^{2+}-doped PEA_2PbBr_4 suggests an equal intensity dopant peak with the host. Whereas in BA_2PbBr_4, at the same Mn^{2+} loading, the intensity of the dopant peak was only ~1/4th of the host peak (Fig. S7, ESI†). Consequently, under the 365 nm excitation, the color of Mn^{2+}:PEA_2PbBr_4 crystals

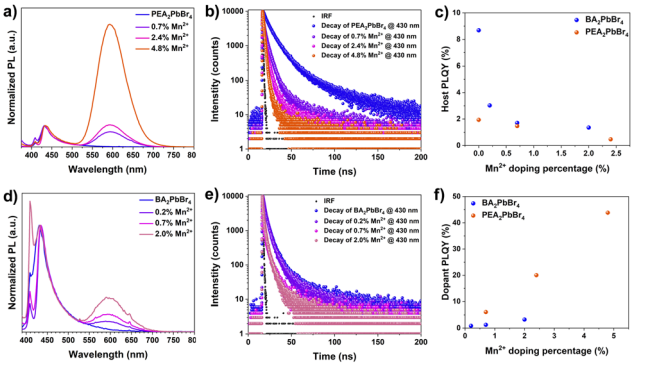

Fig. 3 (a) PL spectra of Mn^{2+}:PEA_2PbBr_4. (b) TRPL of Mn^{2+}:PEA_2PbBr_4. (c) Host PLQY against Mn^{2+} percentage. (d) PL spectra of Mn^{2+}:BA_2PbBr_4. (e) TRPL of Mn^{2+}:BA_2PbBr_4. (f) Dopant PLQY against Mn^{2+} percentage.

appeared significantly different from Mn^{2+}:BA_2PbBr_4 (Fig. S9–S11, ESI†). The emission color tends to move towards orange (λ_{Em} = 600 nm) in Mn^{2+}:PEA_2PbBr_4; however, a more prominent blue emission in Mn^{2+}:BA_2PbBr_4 was observed. These deviations in the PL spectra of Mn^{2+}:BA_2PbBr_4 and Mn^{2+}:PEA_2PbBr_4 crystals show a clear distinction in the CIE 1931 (Commission Internationale de l'Eclairage) chromaticity diagram in Fig. S14 (ESI†).

Furthermore, the time-resolved photoluminescence (TRPL) was recorded at 430 nm and 435 nm for both undoped PEA_2PbBr_4 and BA_2PbBr_4 on the order of nanoseconds (Fig. 3c, and f). The average lifetimes decrease with an increase in Mn^{2+} levels, as shown in Tables S4 and S5 (ESI†). Under the same excitation fluence, the average lifetime of undoped PEA_2PbBr_4 (~8.2 ns) is significantly higher than undoped BA_2PbBr_4 (~3 ns). With a small amount of Mn^{2+} doping, there is a dramatic decrease in the lifetime of the PEA_2PbBr_4 when compared to BA_2PbBr_4, indicating an efficient host-dopant energy transfer in Mn^{2+}:PEA_2PbBr_4. This also complements the intense Mn^{2+} PL in Mn^{2+}:PEA_2PbBr_4 compared to Mn^{2+}:BA_2PbBr_4. Subsequently, the PLQY of the host is decreased (Fig. 3c) and the Mn^{2+} is increased with an increase in the Mn^{2+} doping (Fig. 3f). Both the Mn^{2+} doped 2D perovskites showed a similar decay profile with a prolonged lifetime on the order of microseconds (Fig. S8, ESI†) regardless of the host structure due to the forbidden nature of Mn^{2+} d–d ($^4T_{1g} \rightarrow {}^6A_{1g}$) transitions.[10] As expected, the $PLQY_{Mn}$ of this Mn^{2+} emission at 600 nm increased with an increase in the Mn^{2+} doping in both PEA_2PbBr_4 and BA_2PbBr_4. However, this increase in $PLQY_{Mn}$ is more prominent in PEA_2PbBr_4 compared to BA_2PbBr_4, reaching a maximum of 43.8% (Fig. 3f). From all these studies, it is evident that the host-to-dopant ion energy transfer is more efficient in the case of Mn^{2+}:PEA_2PbBr_4 compared to Mn^{2+}:BA_2PbBr_4. Such differences in optical properties hints towards the important contributions from the nature of doping. In addition, the difference in their crystal phases, and the lattice rigidity due to the difference in their organic spacers may play a critical role in the energy transfer. Regardless, introducing foreign Mn^{2+} ions into the lattice can further perturb the host structure, consequently, the dynamics of exciton transport and the host-to-dopant energy transfer can be affected. After photoexcitation, the excitons generated in the host perovskites diffuse within the inorganic framework before they get

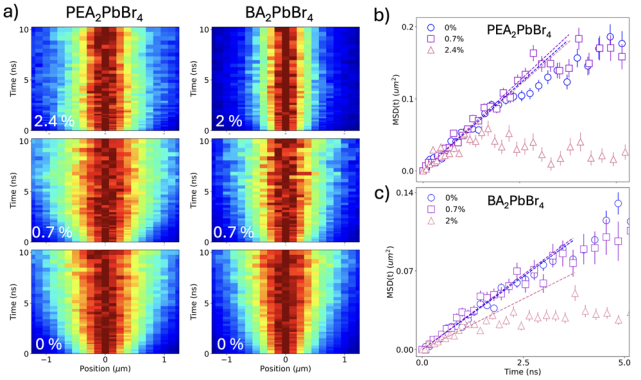

Fig. 4 (a) Diffusion maps of undoped and Mn^{2+} doped PEA_2PbBr_4 and BA_2PbBr_4. The extracted mean-square displacement as a function of time for (b) PEA_2PbBr_4 and (c) BA_2PbBr_4 with different doping levels.

trapped in the Mn^{2+} states. Therefore, the nature of doping, the location of the dopant ions, and strain in the inorganic framework play a critical role in exciton diffusion and energy transport dynamics.[14,15] The efficient host-dopant energy transfer despite the greater strain in Mn^{2+}:PEA_2PbBr_4 perovskites could be due to either (i) the interstitial doping facilitating the smooth sailing of excitons without affecting the landscape of 2D inorganic framework or (ii) the energy transfer barrier for Mn^{2+} may be lower in Mn^{2+}:PEA_2PbBr_4. The weak Mn^{2+} emission in the case of Mn^{2+}:BA_2PbBr_4 perhaps due to the strain created within the inorganic framework due to the lattice contraction by substitutional doping. This strain may be affecting the exciton transport by creating non-radiative defects caused by an inhomogeneous landscape. Consequently, these excitons decay non-radiatively before reaching Mn^{2+} states. Also, the difference in contribution towards the non-radiative sites from rigid aromatic PEA cations and labile aliphatic BA cations cannot be ruled out.

To unveil these dynamics and study the impact of the different doping nature of the two perovskites on exciton transport, we employ TPLM, which allows for direct visualization of in-plane exciton transport. For this, we specifically chose Mn^{2+}-doped PEA_2PbBr_4 and BA_2PbBr_4 with comparable Mn^{2+} doping percentages. Fig. 4a shows the resulting diffusion maps of the undoped and Mn^{2+} doped materials. For both undoped perovskites (Fig. 4a, lower panels), fast spatial expansion of the initial exciton population is observed. In contrast, for doped perovskites, the initial fast diffusion is followed by a stagnation of the expansion, consistent with excitons reaching dopant sites and undergoing energy transfer. We can quantify the rate of expansion by fitting the variance σ of the population for each time slice and calculating the mean-square displacement ($MSD(t) = \sigma_t^2 - \sigma_{0-}$), as shown for the different doping levels in Fig. 4b and c for PEA_2PbBr_4 and BA_2PbBr_4, respectively. From the early time dynamics ($t < 1$ ns), we can extract the diffusivity of the exciton population in the lattice ($MSD = 2D_t$), as indicated by the dashed lines in Fig. 4b and c. For the undoped cases, we observe a higher diffusivity for PEA_2PbBr_4 (0.22 $cm^2\ s^{-1}$) compared to BA_2PbBr_4 (0.13 $cm^2\ s^{-1}$). This is consistent with earlier reports and can be explained by the difference in the softness of the inorganic lattice and a stronger exciton–phonon coupling in BA_2PbBr_4, which slows down transport.[16] Upon doping, it is interesting to note that the diffusivity PEA_2PbBr_4 remains unaffected (Fig. 4b). In contrast, the expansion is notably slower for the highest (2%) doping concentration in BA_2PbBr_4, where the diffusivity drops to 0.08 $cm^2\ s^{-1}$. Interestingly the same sample, BA_2PbBr_4 with 2% Mn^{2+} doping, showed more prominent peak shift in the p-XRD owing to the lattice distortions along the inorganic 2D framework, highlighting the important role of lattice distortions in the exciton diffusion. Further, the lower diffusivity in BA_2PbBr_4 can partially explain the lower PLQY of the Mn^{2+} doping in that system, with slower diffusion leading to less efficient energy transfer.

In conclusion, Mn^{2+} doping induces distinct structural changes by occupying different preferential sites in PEA_2PbBr_4 and BA_2PbBr_4 2D perovskite hosts lattice, interstitial in the former and substitutional in the latter. Interestingly, the resultant crystal shows intense Mn^{2+} emission, which is more efficient in PEA_2PbBr_4 compared to BA_2PbBr_4. The discrepancy in optical properties is most likely due to the nature of doping and its impact on the crystal lattice, including dopant-induced in-plane and out-of-plane lattice strain. Consequently, we observed a striking difference in the exciton diffusion. However, a few aspects like the interstitial site of Mn^{2+} in crystal, the local structure around Mn^{2+} at the interstitial site, and the role of organic spacers require further exploration.

This work was partially funded by the European Union (ERC, EnVision, project number 101125962). FP acknowledges support from the Spanish Ministry of Science and Innovation (CEX2023-001316-M). MG, AS, and UK acknowledge the support from DOE (DE-SC0024214).

Data availability

The data supporting this article have been included as part of the ESI.†

Conflicts of interest

There are no conflicts to declare.

Notes and references

1 M. D. Smith, *et al.*, *Chem. Rev.*, 2019, **119**, 3104–3139.
2 Y. Li, *et al.*, *ChemComm*, 2022, **58**, 941–944.
3 A. J. Torma, *et al.*, *ACS Nano*, 2021, **15**, 20550–20561.
4 S. K. Dutta, *et al.*, *ACS Energy Lett.*, 2019, **4**, 343–351.
5 S. Hou, *et al.*, *Joule*, 2018, **2**, 2421–2433.
6 T. Sheikh and A. Nag, *J. Phys. Chem. C*, 2019, **123**, 9420–9427.
7 F. C. Grozema, *et al.*, *J. Phys. Chem. C*, 2020, **124**, 28201–28209.
8 C. Zhou, *et al.*, *Mater. Sci. Eng., R*, 2019, **137**, 38–65.
9 S. A. Cuthriell, *et al.*, *Adv. Mater.*, 2022, **34**, 2202709.
10 A. Biswas, *et al.*, *Chem. Mater.*, 2017, **29**, 7816–7825.
11 A. Khorsand Zak, *et al.*, *Solid State Sci.*, 2011, **13**, 251–256.
12 R. Kamal Yadav and P. Chauhan, *Indian J. Pure Appl. Phys.*, 2019, **57**, 881–890.
13 T. Jin, *et al.*, *Nat. Commun.*, 2023, **14**, 1–9.
14 D. B. Straus and C. R. Kagan, *J. Phys. Chem. Lett.*, 2018, **9**, 1434–1447.
15 C. M. Mauck and W. A. Tisdale, *Trends Chem.*, 2019, **1**, 380–393.
16 M. Seitz, *et al.*, *Nat. Commun.*, 2020, **11**, 1–8.